Heliyon 10 (2024) e26494

Contents lists available at ScienceDirect

Heliyon

journal homepage: www.cell.com/heliyon

Research article

Chipless RFID based multi-sensor tag for printed electronics

Momina Nadeem, Ayesha Habib *, Mir Yasir Umair

Department of Electrical Engineering, National University of Sciences and Technology, Islamabad 46000, Pakistan

ARTICLE INFO

Keywords:
RFID
Chipless
Moisture sensing
Flexible
Temperature sensing
Sensors
Microwave response
RCS

ABSTRACT

This research presents the design and implementation of a chipless Radio Frequency Identification (RFID) multi-sensor tag on a flexible laminate. Along with the tag's primary function of data encoding for object identification purposes, the tag also incorporates moisture and temperature sensing functionalities within a compact size measuring a mere 15 × 16 mm^2. The tag structure comprises of a total 29 resonators, with each resonator corresponding to one bit in the microwave response. The initial design utilized the bendable Rogers RT/duroid®5880 within a frequency band of 5.48–28.87 GHz. To conduct a comprehensive comparative analysis, the tag design is optimized for two distinct substrates including Kapton®HN and PET. The optimization process involves exploring the utilization of both silver nanoparticle-based ink and Aluminum as radiators. The sensing feature was incorporated by deploying a thin film of Kapton®HN over the longest slot of the tag which acts as a moisture sensor. Temperature sensing feature was achieved by combining Stanyl® polyamide, a temperature dependent polymer, with Rogers RT/duroid®5880 which served as a fused substrate. The tag showcases a high code density of 12.08 bits/cm^2 enabling it to efficiently label 2^{29} unique items. Its unique features include flexibility, miniaturized design, printability, cost-effectiveness and multi sensing property.

1. Introduction

Organic and printed electronics is an emerging area of research spelling huge economic potential for new disruptive technologies. It enables internet-connected electronics to be manufactured as thin, flexible inlays. Such electronics can be applied as labels directly to a product rather than using conventional electronics involving rigid circuit boards. The fast-growing technology enables the production of lightweight and cost-effective electronics that can conform to the curves of an object [1]. The core driver of this market has been the conductive inks which are deposited on different substrates to produce active and passive devices [2]. One of the applications of printed electronics is the printed RFID.

The implementation of RFID technology has brought about a revolutionary transformation in the realms of logistics and retail. It utilizes radio waves to identify and track the movements of goods. An RFID system typically comprises of three fundamental components: a tag to store and transmit information; a reader to interrogate the tag using Radio Frequency (RF) signals; and a database connected to the reader to extract and store data from tag [3]. The main challenge in the wide-scale deployment of RFID in mass-market applications is the higher tag cost since the expense of the identification system relies upon the price of the tag utilized in the system. An alternate remedy to this problem is the elimination of the silicon-chip mounted on the tag. This considerably reduces the system cost giving rise to a new family of RFID tags known as chipless RFID tags. These tags are primarily classified into two categories:

* Corresponding author.
E-mail address: ayesha.habib@mcs.edu.pk (A. Habib).

https://doi.org/10.1016/j.heliyon.2024.e26494
Received 3 July 2023; Received in revised form 13 February 2024; Accepted 14 February 2024
Available online 19 February 2024

Table 1
Comparative analysis of the proposed tag with previously reported chipless RFID tags.

Ref.	Dimension (cm^2)	Bit Capacity (Bits)	Bit Density (Bits/cm^2)	Polarization Insensitive	Printability	Flexibility	Sensing	Frequency Band (GHz)	Year
[19]	6	50	8.33	N/A	Yes	×	×	60	2014
[20]	6.15	13	2.11	Yes	Yes	✓	×	3.1–10.6	2018
[21]	15.6	22	1.41	No	Yes	✓	×	2.4–4.1	2022
[22]	30.25	8	3.90	No	Yes	✓	×	5–13	2019
[23]	1.41	20	15.15	No	Yes	✓	×	3–8	2019
[24]	3.65	10	2.74	Yes	Yes	✓	×	3.6–15.6	2019
[25]	2.6	18	6.92	No	Yes	✓	✓	3.5–16	2022
[26]	2.4	15	6.25	Yes	Yes	✓	×	4.8–18.8	2021
[27]	4.25	12	2.82	No	Yes	×	×	3–6	2019
[28]	5.29	12	2.26	Yes	Yes	✓	×	6.5–18	2021
[29]	4.55	7	1.53	No	No	×	✓	2–8	2021
[30]	9.09	3	0.33	No	No	✓	×	12–17	2022
[31]	2.25	11	4.88	Yes	Yes	✓	×	9.22–18.44	2020
[32]	2.6	6	2.3	Yes	Yes	×	×	4.15–8	2020
[33]	2.46	11	4.46	Yes	Yes	✓	✓	3–6	2021
[34]	1.83	10	5.44	Yes	Yes	✓	×	5.4–10.4	2019
[35]	2.25	5	2.22	No	Yes	×	×	5.5–9.5	2019
[36]	3.44	22	12.79	No	Yes	✓	✓	4–25	2020
[37]	23.52	3	0.127	No	No	×	✓	2.35–2.64	2020
[38]	24.75	6	0.24	No	No	✓	✓	5.3–11	2019
[39]	4.25	20	4.70	No	Yes	✓	✓	4.1–16	2019
[40]	25	21	0.84	No	Yes	×	×	2.2–3.5	2019
[41]	30.58	30	0.99	No	Yes	✓	✓	2.63–9.22	2022
[42]	3.204	32	9.98	Yes	Yes	✓	×	4.5–10.9	2022
[43]	16.66	8	0.48	Yes	Yes	×	×	3–6	2020
[44]	4.06	40	9.85	No	Yes	✓	×	3.1–10.5	2023
This Work	**2.40**	**29**	**12.08**	**No**	**Yes**	✓	✓	**5.48–28.87**	**2023**

active (battery-powered) tags and passive tags [4]. The increasing demand for low-cost and energy efficient tags has caused a fueled growth of deployment of passive chipless RFID tags. Chipless RFID tags have replaced the earlier methods of object identification like barcodes, which held non-modifiable data and relied on a clear LOS and proximity to the scanner for their operation [5]. Such tags impose their unique response on the incoming RF signal and scatter it back towards the reader with some pre-determined frequency.

Embedding sensor functionality in chipless RFID tags further reduces their operational cost [6]. Integration of sensors and RFID tag is attained by making use of substrates that change their electrical properties when subjected to a fluctuation in specific parameters e. g., humidity, Carbon dioxide, pressure, etc. Sensors in RFID tags have revolutionized the process of automatic object identification and monitoring [7]. In literature, various sensor-embedded chipless RFID tags such as humidity sensor [8], accelerometer [9], gas sensor [10], displacement sensor [11], pressure sensor [12], temperature sensor [13], etc. have been reported. In harsh environments, where workers' safety and effective equipment operation are of utmost importance, measuring multi-parameters such as temperature, pressure, and humidity is crucial. Examples include monitoring industrial pipelines [14], preserving flammable and explosive goods [15], and monitoring environmental conditions in mines [16]. Real-time monitoring of temperature, pressure, and humidity is essential for ensuring the safe storage of flammable and explosive materials. However, these monitoring efforts face challenges due to hostile environmental conditions, including airtightness, high temperatures, and the risk of explosions. Conventional wired measures [17,18] have limited use in such situations due to the risk of electric sparks making them unsafe to be utilized in confined spaces. Humidity is another important parameter that can be measured for applications such as food packaging or finding water leakages in buildings. In such situations, the development of wireless and passive measurements has proven to be a promising method for parameter acquisition. Table 1 demonstrates the motivation behind the formulation of the proposed tag by providing a comparison with previously published chipless RFID tags in literature.

This research presents the design and analysis of a novel data-dense, miniaturized, fully printable multi-sensor RFID tag for data encoding and sensing purposes. The tag was first developed using a bendable substrate, i.e., Rogers RT/duroid®5880, with copper resonators having a compact dimension measuring 15 × 16 mm^2 in size. Subsequently, the tag was evaluated on other flexible substrates that include PET (Polyethylene Terephthalate) and Kapton®HN. The slot-resonator geometry of the tag encodes 29 bits that correspond to 29 slots in the tag structure. The tag has a pentagonal structure that is divided into 14 H-polarized slots and 15 V-polarized slots by metal radiators. The additional built-in multi-sensing feature is obtained by using humidity sensitive substrate Kapton®HN, and a temperature dependent polymer, Stanyl® polyamide. The novel aspects of this research include its compact design, ease of fabrication, multi-sensing nature, high data encoding capacity, and identification of 2^{29} unique items.

2. Theoretical framework

The proposed tag is a backscattered-based tag that uses the backscattering phenomenon to communicate data wirelessly between the tag and the reader. The key benefit of this approach is that no antennas are required for the operation [45], which results in a smaller tag size. The chipless RFID tags that rely on backscattering principle do not require any communication protocol [46]. The reader interrogates the tag by transmitting an RF wave toward it. The instantaneous E-field of the incident plane wave is expressed by eq. (1).

$$(Z,t) = a_x Re\left[E_{x0}e^{j(\omega t+kz+\varphi x)}\right] + a_y Re\left[E_{y0}e^{j(\omega t+kz+\varphi y)}\right] \quad (1)$$

In the above equation, the electric field is denoted by E, time by t, wave vector by k, the angular frequency of the wave by ω, and the position vector by (x,y,z).

The tag extracts power from this RF signal, implies its specific response on the incident signal, and then scatters an encoded electromagnetic (EM) signal back toward the reader. The reader uses this backscattered signal to retrieve information about the remotely placed object. Fig. 1 illustrates the operational principle of backscattered-based tags. The distinctive frequency signature

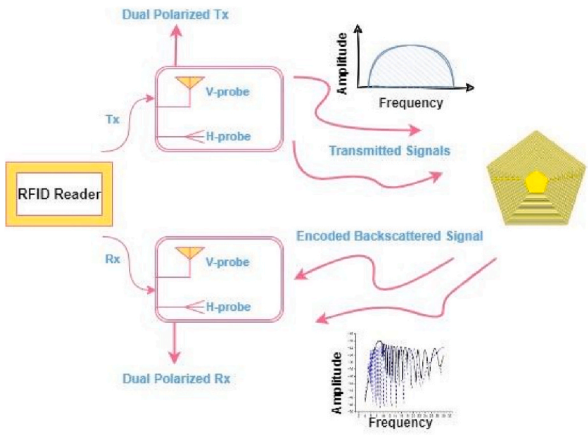

Fig. 1. Backscattering technique in chipless RFID.

present in the backscattered response of the tag signifies the unique tag ID for the identification process. The Radar Cross-Section (RCS) parameter can be employed to evaluate the response of the tag [47].

Eq. (2) describes the relationship between the RCS response of the tag and the intensities of the scattered electric field (E_{scat}) and incident electric field (E_{inc}) [48].

$$\sigma = \lim_{r\to\infty}\left[4\pi r^2.\frac{|E_{scat}|^2}{|E_{inc}|^2}\right] \tag{2}$$

where σ represents the RCS curve magnitude and r denotes the distance between the reader and the tag. Another approach to obtain the RCS response of a tag is by measuring the power received by the tag (Pr) from the reader and employing the radar range equation to calculate the RCS [49–51]. This is shown in eq. (3), and (4).

$$P_r = \frac{P_t G_t P_t \lambda^2 \sigma}{(4\pi)^3 R^4} \tag{3}$$

$$\sigma_{target} = \frac{(4\pi)^3 R^4 P_r}{P_t G_t G_r \lambda^2} \tag{4}$$

In these equations, the power levels of transmitting and receiving antennas are denoted by P_t and P_r, their respective gains by Gt and G_r, operating wavelength by λ, and the read range of the tag by R. The slot-resonator geometry on the surface of the tag facilitates the backscattering process by tuning each resonant element to resonate at a unique frequency [23]. Within this structure, each slot is linked to a distinct dip in the frequency response of the tag, where each dip represents a single bit. The relationship between resonant frequencies corresponding to a particular slot is given by eq. (5).

$$fr \approx^{c} \frac{2}{L\sqrt{\varepsilon_r}} \tag{5}$$

$$where\ \varepsilon_{eff}\frac{1+\varepsilon r}{2}$$

In eq. (5), the speed of light is represented by $c = 3 \times 10^8$, the slot length is denoted by L, the effective permittivity is indicated by ε_{eff}, and the relative permittivity of the substrate is represented by ε_r. However, this equation does not account for the influence of slot width and substrate thickness on the resonant frequency.

3.Proposed tag development

The simulation software CST Microwave Studio Suite® is utilized to evaluate the electromagnetic behavior of the 29-bit tag with a pentagonal slot-resonator-based geometry. The slots are divided by metal radiators to increase the data density of the tag and to achieve 29 slots that correspond to 29 unique frequencies in the RCS response of the tag. A frequency dip within the tag's response signifies a logic state '1′, whereas the absence of a dip indicates a logic state '0'. Since RCS is a far-field parameter, the tag must be positioned at a distance, r, within the far-field, as determined by eq. (6).

$$r \geq \frac{2D^2}{\lambda} \tag{6}$$

The eq. (6) provides the far-field distance for observing the RCS, and it is defined as a function of the largest dimension D of the radiating structure and the wavelength λ of the EM wave.

Fig. 2 showcases the configuration of the tag in the simulation setup. To receive and analyze the backscattered signal from the tag, both the E-field (far-field) and RCS probes are positioned at a precise distance of 40 mm within the far-field region. The dual-polarized

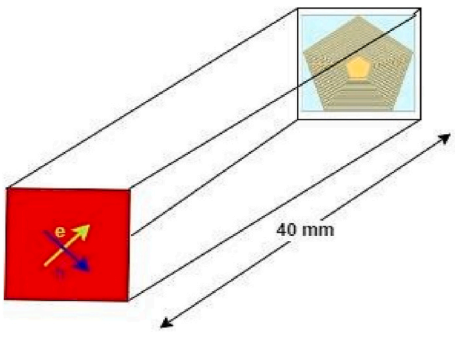

Fig. 2. Simulation setup for the proposed Tag.

tag has 14-horizontally polarized slots and 15-vertically polarized slots and thus requires a linearly dual-polarized plane wave for its operation. The design flow of the proposed tag is presented in Fig. 3.

The fabrication of the proposed 29-bit tag is carried out on the ungrounded Rogers RT/duroid®5880 substrate, employing a copper layer with a height of r = 0.35 mm. This design enables the tag to be read from both the front and back sides. The substrate possesses a relative permittivity of $\varepsilon_r = 2.2$, a thickness of h = 0.508 mm, and a low loss tangent of tan δ = 0.0009. The tag is designed to function within a frequency range of 5.48–28.87 GHz. The geometry of the proposed tag is demonstrated in Fig. 4 (a) and its cross-sectional view is illustrated in Fig. 4 (b).

The tag structure comprises of 29 resonators each of varying lengths within a compact area of 2.4 cm^2, where the length is L = 16 mm, and the width is W = 15 mm. To avoid mutual coupling between the adjacent slots from S_1 to $S_{29,}$ a uniform distance g, has been maintained irrespective of the sharper resonances, the distance g can be altered.

The tag is partitioned into two portions, namely R_1 and R_2, with widths of 0.2 mm and 0.15 mm, respectively. The lower portion of the tag corresponds to 14-horizontally polarized slots and the upper portion along with one pentagonal slot at the center corresponds to the 15- vertically polarized slots. The length of each slot is different from the others; therefore, a unique frequency signature is obtained. One of the motivations behind this tag structure is its simple design and easy printability. Table 2 summarizes the optimized design parameters for the tag.

When the reader emits an RF wave toward the tag, an EM wave propagates in the structure. This induces current distribution in the tag and excites it. The current distribution of the smallest slot has been simulated and shown in Fig. 5. A depiction of the tag structure along with its equivalent circuit is provided in Fig. 6(a) that showcases the LC circuit of the tag.

When plotted, the increasing capacitance and decreasing inductance in the series RLC circuit cross each other at 'fr' as depicted in Fig. 6(b). At this point, the inductance and capacitance achieve equivalence (XL = XC), and the circuit resonates at a specific resonant frequency given by eq. (7).

$$fr = \frac{1}{2\pi\sqrt{LC}} \tag{7}$$

In the above equation, *fr* represents the resonant frequency, *L* denotes the inductance and *C* signifies the capacitance of the circuit.

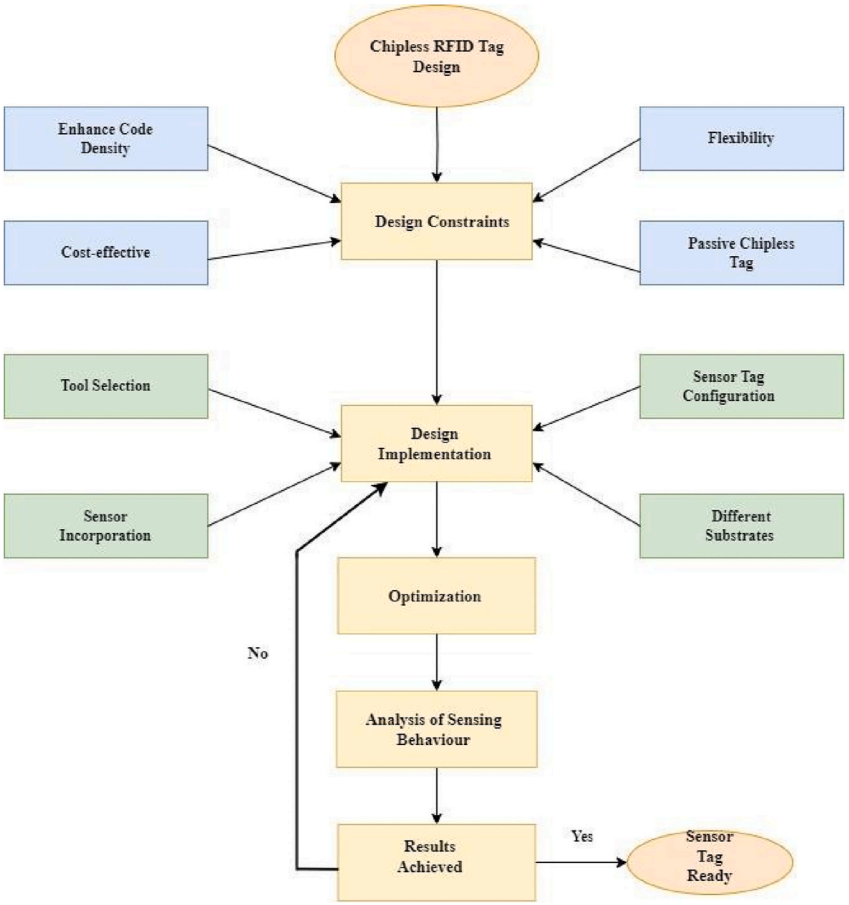

Fig. 3. Design flow of the proposed sensor Tag.

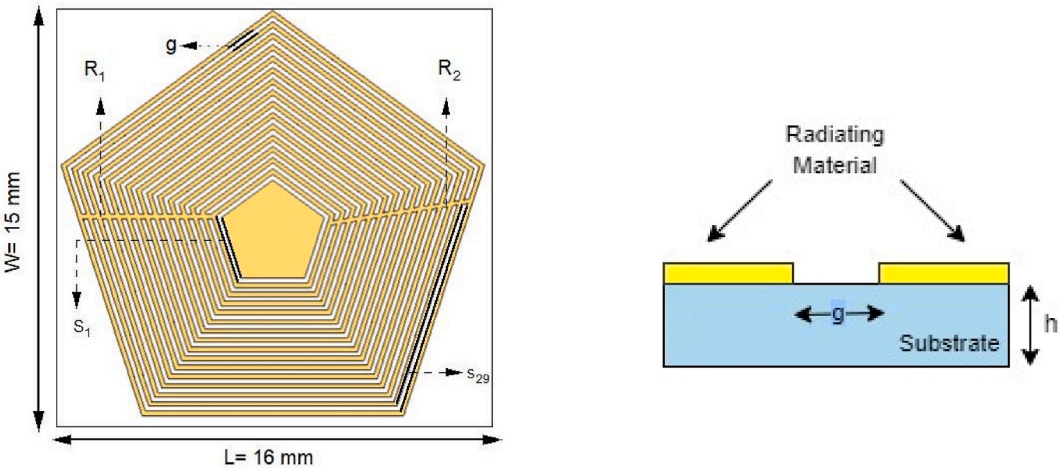

Fig. 4. (a) Layout of the proposed tag (b) Cross-sectional view of the tag.

Table 2
Design parameters for the proposed tag.

Parameter	Dimension (mm)	Parameter	Dimension (mm)
L	16	*S13*	14.55
W	15	*S14*	17.04
G	0.2	*S15*	13.42
R1	0.2	*S16*	15.83
R2	0.15	*S17*	12.24
S1	21.57	*S18*	14.58
S2	24.48	*S19*	11.07
S3	20.40	*S20*	13.34
S4	23.24	*S21*	9.90
S5	19.26	*S22*	12.11
S6	22.03	*S23*	8.74
S7	18.06	*S24*	10.87
S8	20.76	*S25*	7.56
S9	16.89	*S26*	9.62
S10	19.52	*S27*	6.43
S11	15.73	*S28*	8.41
S12	18.28	*S29*	12.81

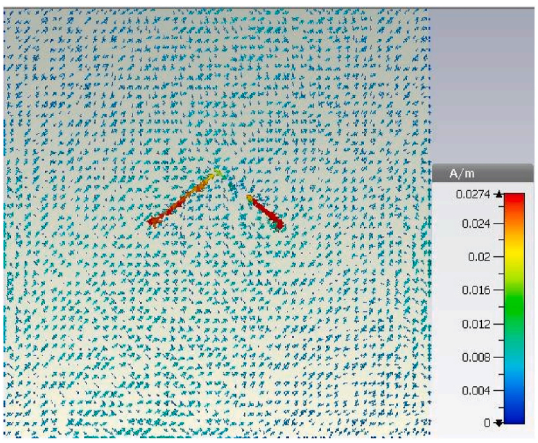

Fig. 5. Surface current distribution of the slot resonating at 28.87 GHz.

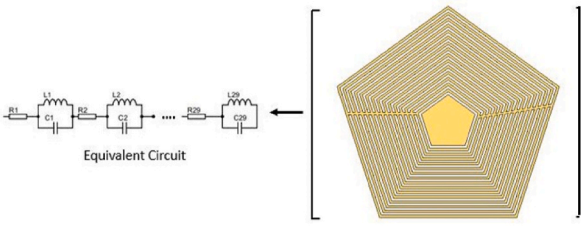

(a)

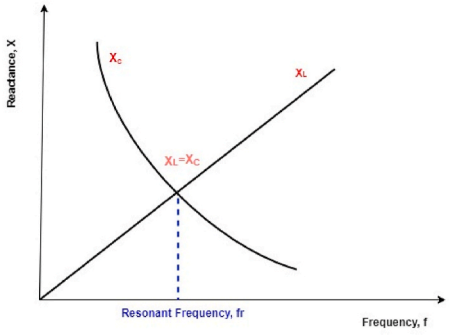

(b)

Fig. 6. (a) The equivalent circuit of the tag (b) Reactance vs. Frequency plot for LC circuit of one slot.

The proposed tag's performance is tested and validated using an experimental setup utilized in Ref. [52]. In this configuration, a Vector Network Analyzer (VNA) having two ports is employed, with each port connected to a pair of identical horn antennas. One antenna functions as the transmitter, while the other acts as the receiver. The transmitter emits EM waves towards the tag, which is affixed to a box, as depicted in Fig. 7. The tag is positioned in the far-field region relative to the horn antennas. The transmitted EM waves interact with the tag, which reflects its unique response onto the incident plane wave directed towards the receiver. The receiver captures the backscattered encoded signal and feeds it to the VNA, which analyzes the transmitted and received response. Throughout the measurement process, a transmit power of 0 dBm is utilized within the operational frequency band.

There are two kinds of $S11$ parameters that are measured while measuring the RCS response of the tag i.e., S isolation which is measured when chipless tag is not present, and S ^{ref} which is measured when the chipless tag is present. Eq. (8) [53] can be used to estimate the RCS value.

$$\sigma^{tag} = \left[\frac{S11^{tag} - S11^{isolation}}{S11^{ref} - S11^{isolation}}\right]\sigma ref\,(dBsm) \tag{8}$$

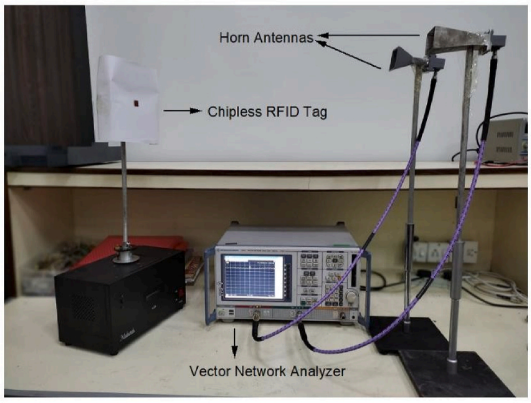

Fig. 7. Measurement setup for the proposed chipless tag.

Where σ^{ref} denotes the RCS response of the proposed tag and is given by eq. (9).

$$\sigma^{ref} = \left[\frac{Area\ of\ plate}{\lambda}\right]^2 4\pi \tag{9}$$

The comparison of results obtained from simulations and measurements across H- probe and V-probe are presented in Fig. 8 (a) and Fig. 8 (b), respectively. It can be observed that the computed and measured results exhibit a notable level of agreement.

The measured results show a small deviation in the dips of certain resonant frequencies. This is due to environmental factors and subtle design disabilities during the fabrication process.

4. Tag performance analysis

Ideally to develop a low-cost and easily printable tag, the tag design mechanism should be kept uncomplicated. With this perspective, the chipless RFID tag has been meticulously designed using various substrates and conducting materials. Initially, Tag-A was developed utilizing the flexible Rogers RT/duroid®5880 substrate with copper resonators that are 0.35 mm thick. Fig. 9 displays the RCS response of the Tag-A. Each dip in the 23.39 GHz frequency range corresponds to '1′ bit in the Tag ID. The Most Significant Bit (MSB) exhibits resonance at 5.48 GHz, while the Least Significant Bit (LSB) resonates at 28.87 GHz. Among the 29 bits generated by the tag, fourteen bits are observed through the upper slots, which are excited by horizontally polarized incident plane waves, while the remaining fifteen bits are observed through the lower slots, energized by vertically polarized RF waves.

The identical tag design has been optimized for substrates made from flexible and recyclable materials, employing organic conductive inks. The tag is designed on a Kapton®HN substrate, utilizing two distinct conductive materials: silver nano-ink and aluminum [54].

The proposed tag offers customization, allowing for the encoding of unique data words during the fabrication process. By introducing or removing slots within the design, an impressive array of 2^{29} distinct tags can be generated. Fig. 10 serves as a visual representation of three tag variants. The first variant signifies an all-ones configuration, corresponding to a data word of 11111111111111111111111111111. The second variant showcases an all-zero configuration, reflecting a data word of 00000000000000000000000000000. Lastly, the third variant displays a random sequence with a data word of 10010010100110011000100010101. Each of these variants is presented alongside its physically modified structure, illustrating how the addition or removal of slots results in distinct encoding patterns. These structural modifications directly align with the represented data words. In Fig. 10(a), no slots have been shorted. In Fig. 10(b), all slots within the tag are shorted by filling the substrate material within them. In Fig. 10(c), specific slots numbered 2, 4, 6, 7, 8, 11, 12, 15, 16, 19, 20, 22, 24, 25, 27, and 28 are shorted. The presence of shorted slots corresponds to observable flat dips in the respective RCS response at those particular frequencies.

Tag-B is evaluated by employing Kapton®HN substrate and an Aluminum metal radiator with a thickness of 0.007 mm. The substrate itself has a thickness of 0.125 mm, a permittivity value of 3.5, and a loss tangent of 0.0026. In Fig. 11, RCS response of Tag-B is depicted for an all-ones ID combination. The operational frequency range for this tag spans from 5.56 GHz to 28.75 GHz, where the MSB and LSB resonate at 5.56 GHz and 28.75 GHz, respectively.

Fig. 12 presents the RCS curve of Tag-B' which is designed using the same Kapton®HN substrate with conductive traces made by the silver nano-particle-based ink of thickness 0.015 mm. This tag yields 29 bits within a bandwidth of 23.07 GHz with MSB and LSB at 5.50 GHz and 28.81 GHz, respectively.

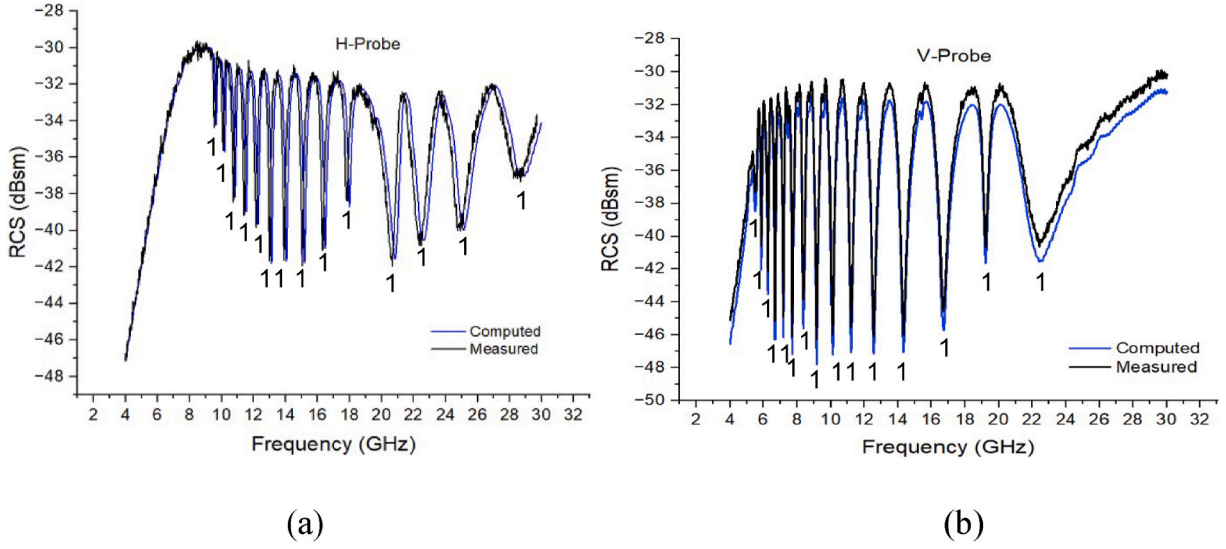

Fig. 8. (a) Computed and measured H-probe results (b) Computed and measured V-probe results.

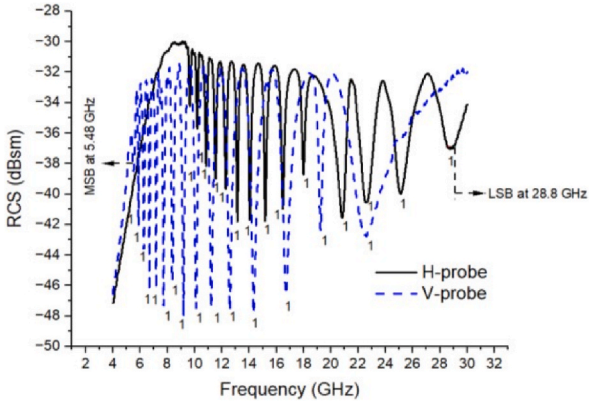

Fig. 9. Tag-A backscattered response.

To further analyze the performance of Tag-C and Tag-C′ on different substrates, a thin and flexible PET substrate is utilized, along with Aluminum and Silver nano-particle-based ink as radiators, respectively. The PET substrate has a thickness of 0.1 mm and exhibits an electric permittivity value of 3.3, along with a loss tangent of 0.003. The conducting material used for Tag-C is Aluminum having thickness 0.007 mm. Fig. 13 illustrates the overall bandwidth possessed by Tag-C which is 23.32 GHz with MSB at 5.50 GHz and LSB at 28.82 GHz.

The frequency response of Tag-C′ is illustrated in Fig. 14, showcasing RCS in relation to the frequency. This tag is fabricated using a PET substrate and utilizes silver nano-particle-based ink as the radiating material. To simplify the fabrication process, the Aluminum metal is replaced with a conductive ink that has a thickness of 0.015 mm and exhibits good electrical conductivity i.e., 9×10^6 S/m. Tag-C' covers a bandwidth ranging from 5.73 GHz to 29.73 GHz. A comparison of the characteristics of the proposed tags is presented in Table 3.

5. Chipless RFID sensor designing

Due to their high cost, discrete environmental sensors are unsuitable for large-scale deployment. However, the integration of chipless RFID tags with sensors offers a cost-effective solution for widespread sensing applications. Such sensing tags are designed by using substrates that change their electrical properties when subjected to a change in certain environmental parameters [55].

a. Humidity Sensing Performance

To incorporate humidity sensing feature within the proposed tag, Kapton®HN can either be used as a substrate or placed over a specific slot in the tag structure. In this research, a thin film of Kapton®HN having thickness of 0.1 mm is deposited over the longest slot of Tag-A resonating at. 5.48 GHz as illustrated in Fig. 15. The sensing bit is associated with the MSB of the tag and the remaining 28 slots are being used for data encoding purposes. The Kapton film is capable of absorbing moisture from the surrounding atmosphere and alters its electrical properties which results in a shift in the overall frequency band of the tag [54,55].

Kapton®HN is a hygroscopic polymer which exhibits a linear change in its dielectric permittivity in response to variations in relative humidity (RH). From its data sheet [56], it is known that the dissipation factor of Kapton®HN varies from 0.0015 at 0% RH to 0.0035 at 100% RH. This property of Kapton®HN is demonstrated by eq. (10).

$$\varepsilon_r = 3.05 + 0.008 \times RH\% \tag{10}$$

Refer to the chemical structure of Kapton®HN (C12H12N2O) illustrated in Fig. 16. When water is absorbed between the free spaces in the structure of Kapton®HN, a hydrolysis process occurs.

This causes a variation of internal electric polarization due to the breakdown of carbon-nitrogen bonds. The absorption of humidity by the polymer alters the permittivity of Kapton®HN molecule which is directly proportional to the quantity of water absorbed [33]. The alteration in permittivity causes a modification in the electrical polarization, leading to a shift in the resonant frequency. This feature of the Kapton®HN polyamide makes it very suitable for use in cold storages (food industry), drug storage, and other moisture sensitive applications.

The shifting of the resonance associated with the sensing slot of the tag in presence of moisture is quantified as humidity sensing. In Fig. 17, the humidity sensing characteristics of the tag on H-probe are demonstrated at various humidity levels (30%, 50%, and 80%). The results indicate that as the relative humidity (RH) increases, the permittivity of Kapton®HN shifts from 3.3 to 3.7. Consequently, the resonant frequency of the sensing slot also shifts towards lower frequencies.

For a 20% rise in RH value from 30% to 50%, there is a shift of 77.2 MHz, and for a rise of 20% in the humidity level from 50% to 80%, a frequency shift of 51.5 MHz towards the left side is observed in the RCS curve. It is important to highlight that this alteration in the resonating frequency of the sensing slot does not impact the number of bits generated by the tag. Fig. 18 highlights that the tag

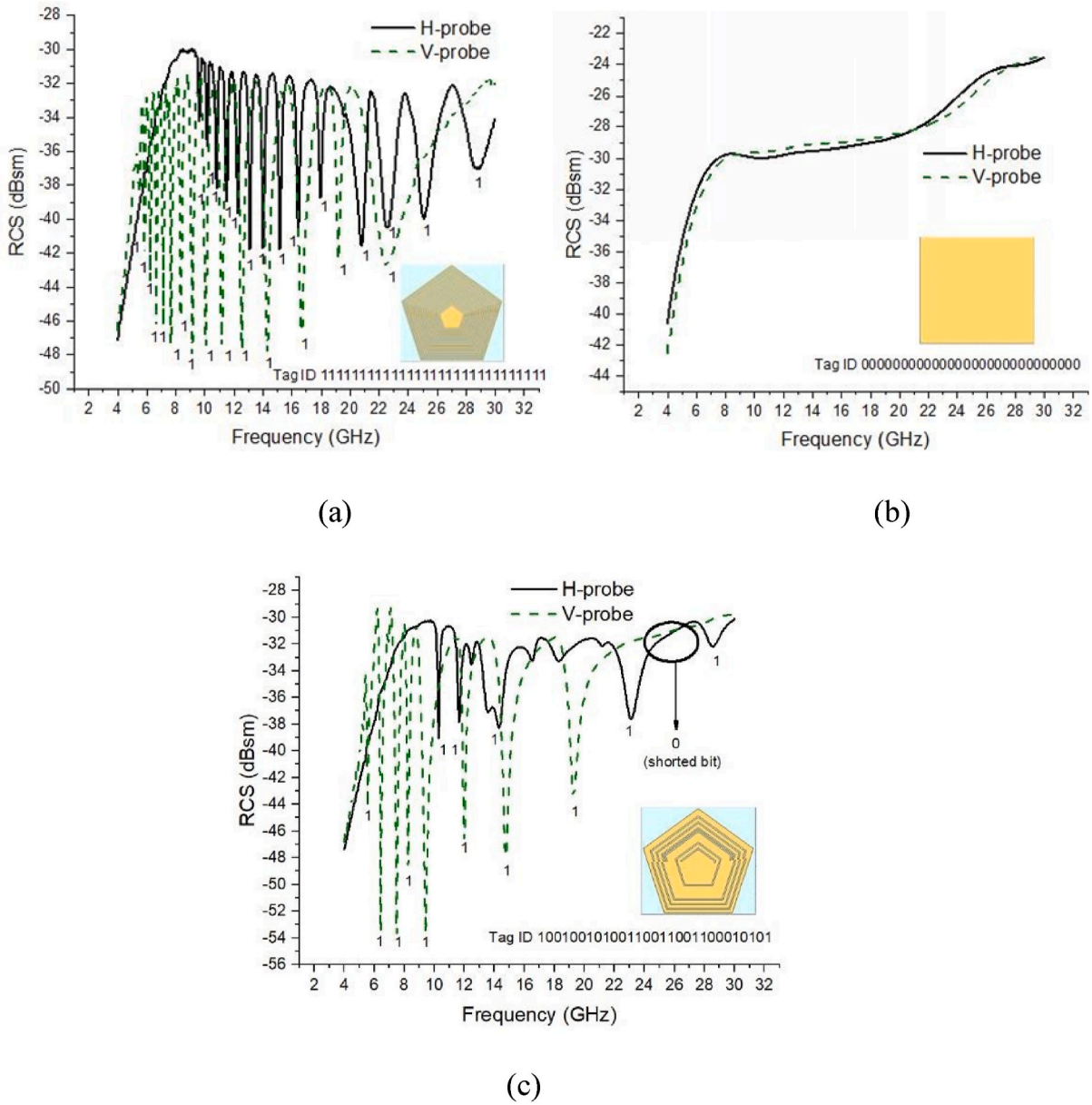

Fig. 10. (a) RCS and tag design for data word 11111111111111111111111111111111 (b) RCS and tag structure for data word 00000000000000000000000000000000 (c) RCS and tag design for data word 10010010100110011000100010101.

showcases a tolerance level of 0.1% within the specified RF band and 0.2% along the RCS axis. This observation significantly bolsters confidence in the reliability of the suggested tag.

The measurement of the proposed humidity RFID sensor tag's response is conducted using a setup outlined in Ref. [6]. This setup includes an environmental chamber with dimensions of 50 × 34 × 36 cm^3, two horn antennas, a water spray bottle, a commercial sensor, and the proposed sensor. To obtain the measured results at room temperature, a VNA is positioned near the environmental chamber. Within the chamber, the horn antennas and sensor are placed 20 cm above the box's bottom, while the proposed humidity sensor tag is positioned at a far-field distance of 40 mm from the horn antennas. The RCS is determined using eq. (8). Fig. 19 illustrates the humidity response of the proposed sensor, showcasing measurements taken along both vertical and horizontal probes. The measurement process involves spraying water inside an airtight chamber and subsequently closing the lid for a duration of 10 min.

To obtain measured results with RH levels 30%, 50% and 80%, the water is sprayed within the chamber at regular intervals. Hence, there is a fluctuation in the moisture level within the chamber. This makes the thin Kapton®HN tape deposited on the longest slot of the tag alter its electrical properties causing the MSB to drift towards lower frequencies in the RCS response. The ripples in the measured response depict the effect of environmental factors. It is observed that there is an overall shift of 128.7 MHz from 8.57 to 8.44 GHz

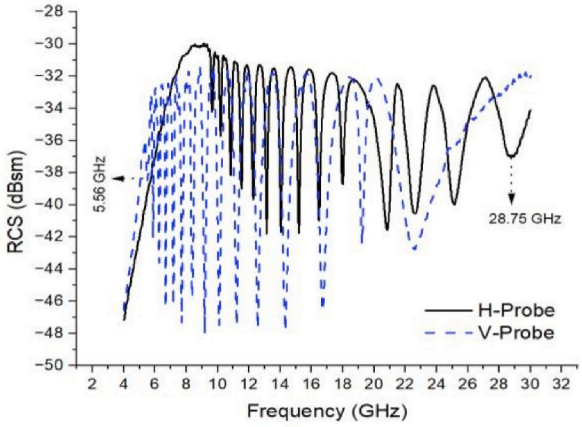

Fig. 11. Tag-B backscattered response.

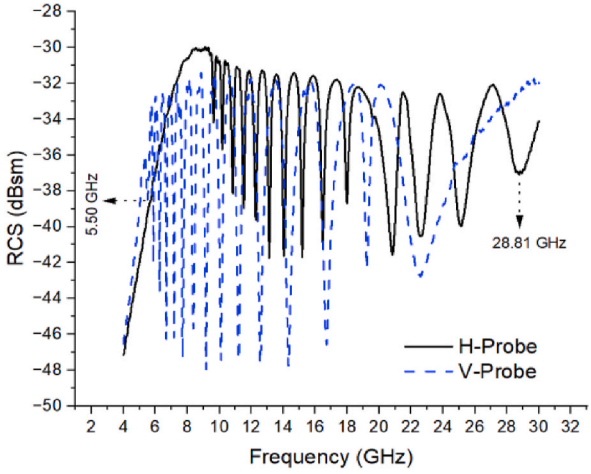

Fig. 12. Tag-B′ backscattered response.

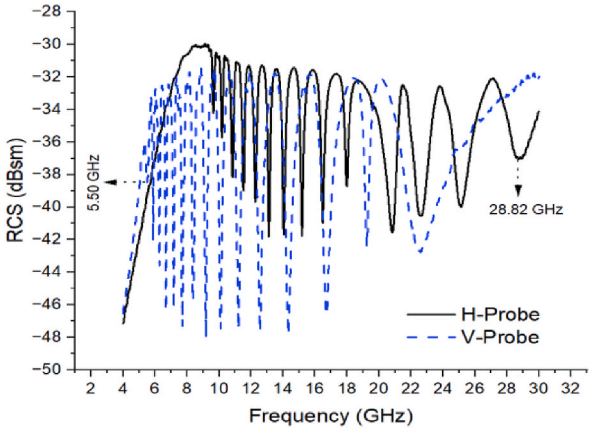

Fig. 13. Tag-C backscattered response.

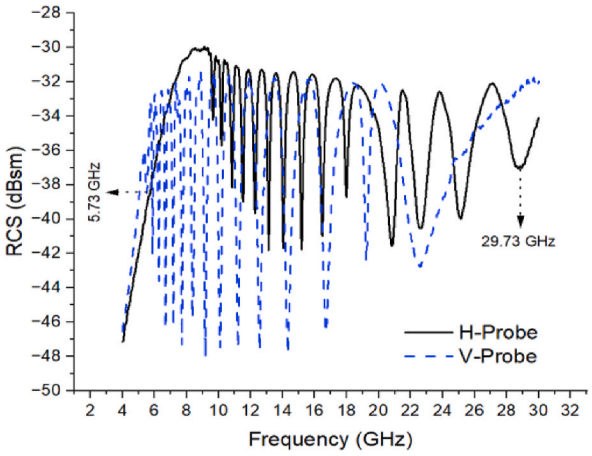

Fig. 14. Tag-C′ backscattered response.

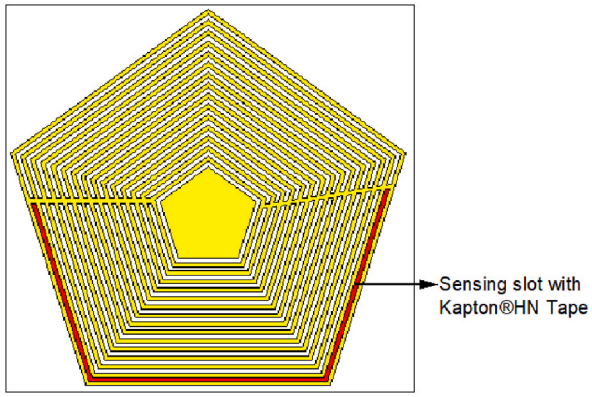

Fig. 15. Rogers RT/duroid® 5880 Tag with Kapton®HN film deposited on the longest slot.

Table 3
Comparative analysis of proposed tags.

Parameters	Tag-A	Tag-B	Tag-B′	Tag-C	Tag-C′
Substrate	Rogers RT/duroid/5880	Kapton®HN	Kapton®HN	PET	PET
Thickness (mm)	0.508	0.125	0.125	0.1	0.1
Permittivity	2.2	3.5	3.5	3.3	3.3
Loss Tangent	0.0009	0.0026	0.0026	0.003	0.003
Radiator	Copper	Aluminum	Silver Ink	Aluminum	Silver Ink
Rad. Thickness (mm)	0.35	0.007	0.015	0.007	0.015
Conductivity (S/m)	–	3.5×10^7	9×10^6	3.5×10^7	9×10^6
Transmission bits	29	29	29	29	29
Freq. Band (GHz)	5.48–28.87	5.56–28.75	5.50–28.81	5.50–28.82	5.73–29.73
Bandwidth (GHz)	23.39	23.19	23.07	23.32	24

when relative humidity increases up to 80%.

a Temperature Sensing Performance

The proposed chipless design has also achieved temperature sensing functionality by incorporating temperature-sensitive material into a single bit of the tag. To incorporate temperature sensing, structural modification has been carried out within the tag architecture. A temperature-dependent polyamide, Stanyl®TE200F6 polyamide, is filled inside the longest slot of the tag as portrayed in Fig. 20 (a). Fig. 20 (b) visualizes the tag from the rear side. Stanyl® polyamide, known for its thermal expansion coefficient of (0.2×10^{-4} ppm/°C) [57], exhibits excellent resilience under extreme temperatures and harsh environments, making it capable of withstanding high stress and heavy loads.

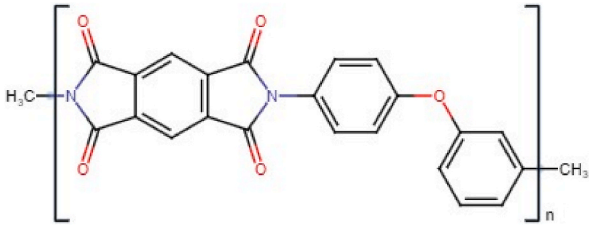

Fig. 16. Chemical structure of Kapton®HN.

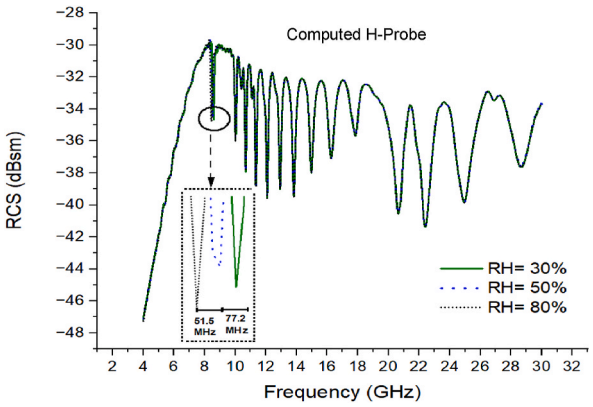

Fig. 17. Computed humidity sensing behavior.

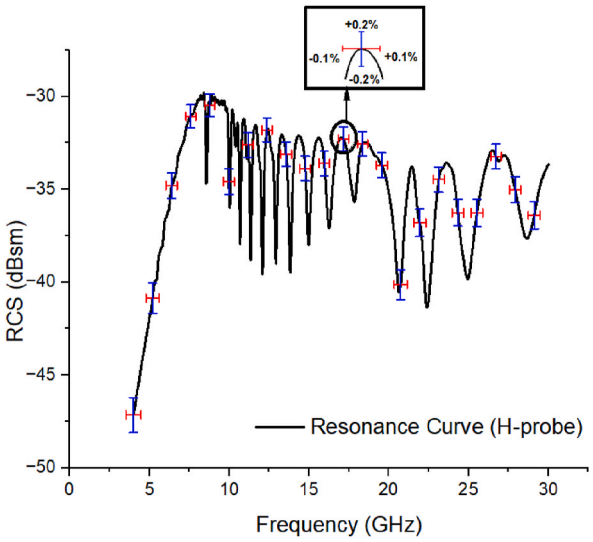

Fig. 18. Reliability curve of humidity sensor (H-probe).

A slice equal to the length of the longest slot is cut away from the Rogers RT/duroid® 5880 substrate and replaced with Stanyl®. This impact is limited to the lowest resonant frequency within the tag's frequency signature. The adjacent resonant frequencies remain unaffected and retain their function of data encoding. Fig. 21 shows that as the relative permittivity, ε_r, increases from 3.5 to 3.8 due to temperature elevation, a slight drift of 79.8 MHz towards lower frequencies is observed in the resonant frequency of the sensing slot. The sensing information is retrieved from the shifting of the lower resonant frequency. The obtained results show an inverse correlation between the resonant frequency and temperature.

Fig. 22 presents an analysis of the relationship between dielectric constant and the temperature. Based on the results, it can be observed that the Stanyl® polyamide exhibits a linear change in its dielectric constant as the temperature varies [58]. Consequently, the effective relative permittivity of the tag undergoes a change, leading to a shift in its frequency response.

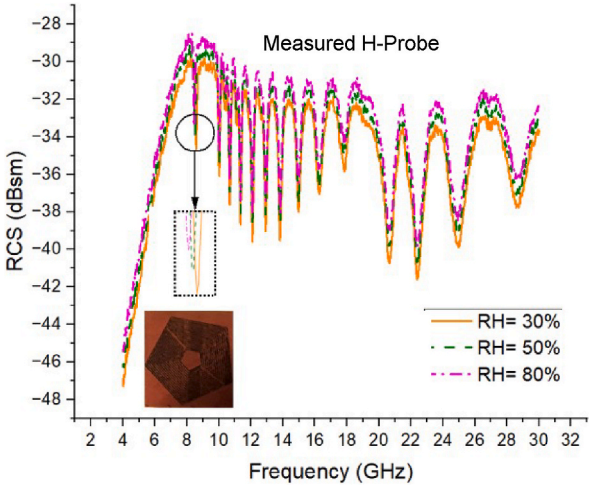

Fig. 19. Measured results of the humidity sensor.

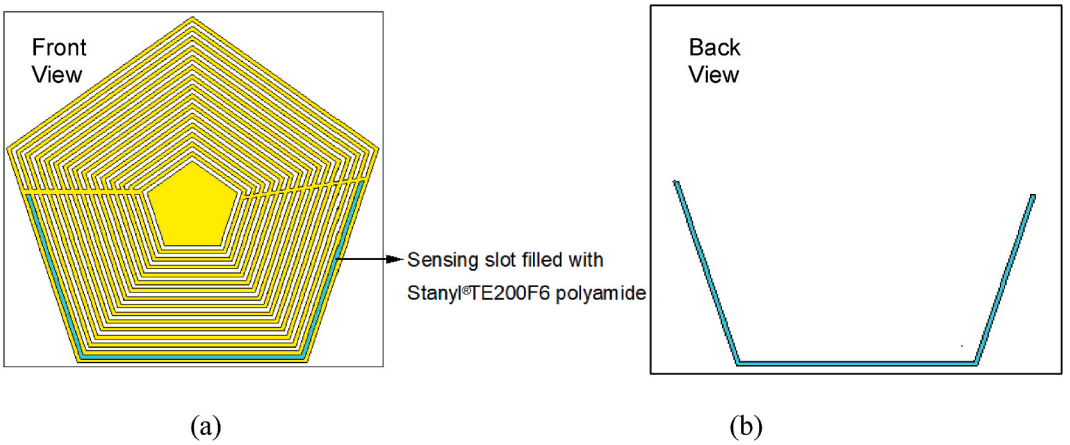

Fig. 20. (a) Front-view of temperature sensing tag (b) Back-view of temperature sensing tag.

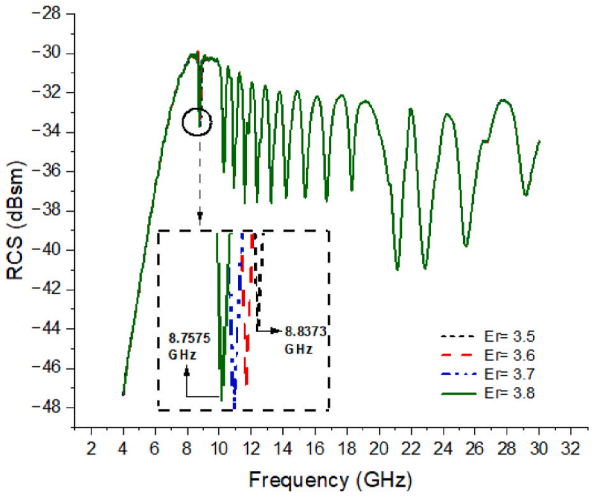

Fig. 21. Temperature sensing behavior of the proposed sensor tag with Stanyl®TE200F6 polyamide.

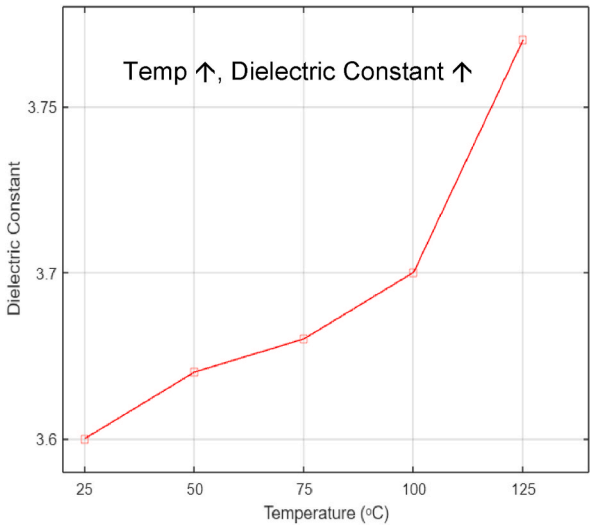

Fig. 22. Relationship between dielectric constant of Stanyl®TE200F6 and temperature.

6. Conclusion

A novel chipless RFID sensor tag is discussed in this journal. The sensor tag uses frequency domain-based encoding to enable the tagging of $2^{29} = 536{,}870{,}912$ items. The tag has been meticulously engineered to possess a compact size, measuring 15×16 mm^2 in dimensions. Furthermore, a comprehensive analysis of the tag has been conducted, taking into account its performance across three distinct substrates: Rogers RT/duroid/5880, Kapton® HN, and PET. These substrates have been selected to provide a thorough understanding of the tag's behavior and suitability in various operating conditions. The tag referred to as Tag-A is designed using Rogers RT/duroid®5880 substrate with copper as the conducting material on its surface. It exhibits flexibility and yields 29 bits in the frequency band of 5.48–28.87 GHz. Tag-B and Tag-B′ are developed on the flexible Kapton®HN substrate with Aluminum and silver nanoparticle-based ink as radiators, respectively. Tag-C and Tag-C′ utilize the flexible PET substrate with Aluminum and silver ink as the radiating materials, respectively. Tag-C operates in the frequency band of 5.50–28.82 GHz while Tag-C′ has a bandwidth of 24 GHz. All tag designs have the ability to encode 29 bits. In addition to its basic function of data storage, the tag incorporates features for humidity and temperature sensing. This is achieved by utilizing moisture-sensitive tape to monitor humidity levels and integrating heat-sensitive Stanyl® polyamide to sense temperature fluctuations. By employing moisture sensitive Kapton®HN tape over the longest slot of the tag, the tag is equipped to detect humidity levels in its surroundings. The humidity sensing behavior of the tag is evaluated for different humidity levels i.e., 30%, 50% and 80%. The results show that with an increase in the relative humidity, the relative permittivity of the Kapton®HN substrate changes, which causes the resonant frequency of the sensing slot to shift towards the lower frequencies. There is an overall shift of 128.7 MHz for the said humidity levels. This capability proves invaluable in applications where maintaining optimal humidity conditions is critical, such as in the storage of sensitive electronic components or perishable goods. The tag's temperature sensing functionality is achieved through the integration of Stanyl® polyamide into the longest slot of the tag. As the temperature increases, there is an increase in the relative permittivity of Stanyl®. This change in the permittivity causes the frequency dip of the sensing slot to drift 79.8 MHz towards the lower frequencies. This sensing behavior of the tag is observed in the MSB of the RCS response. It makes the tag ideal for applications where temperature control is vital, such as cold chain logistics or temperature-sensitive manufacturing processes. By incorporating both humidity and temperature sensing capabilities into the tag, it transforms into a versatile and comprehensive monitoring solution. Hence, the tag not only stores essential data but also provides valuable insights into the environmental conditions it operates within, ensuring optimal conditions and enhancing overall operational efficiency.

CRediT authorship contribution statement

Momina Nadeem: Writing – original draft, Software. **Ayesha Habib:** Writing – review & editing, Supervision, Methodology, Formal analysis, Conceptualization. **Mir Yasir Umair:** Project administration, Investigation.

Declaration of competing interest

The authors declare that they have no known competing financial interests or personal relationships that could have appeared to influence the work reported in this paper.

References

[1] Technology status and application development, ESSCIRC 2008-34th European Solid-State Circuits Conference, IEEE, 2008.
[2] Yasser Khan, Arno Thielens, Sifat Muin, Jonathan Ting, Carol Baumbauer, Ana Arias, A new frontier ofed electronics: flexible hybrid electronics, Adv. Mater. 32 (2020), https://doi.org/10.1002/adma.201905279.
[3] M.A. Islam, N.C. Karmakar, Compact printable chipless RFID systems, IEEE Trans. Microw. Theor. Tech. 63 (11) (Nov. 2015) 3785–3793, https://doi.org/10.1109/TMTT.2015.2482968.
[4] H.E.L. Matbouly, S. Tedjini, K. Zannas, Y. Duroc, Chipless sensing system compliant with the standard radio frequency regulations, IEEE Radio Freq. Identification J. 3 (2) (2019) 83–90. https://doi:10.1109/JRFID.2019.2909092.
[5] F. Salemi, H.R. Hassani, S. Mohammad-Ali-Nezhad, Linearly polarized compact extended U-shaped chipless RFID tag, AEU – Int. J. Electron. Commun. 117 (2020) 153129–153136, https://doi.org/10.1016/j.aeue.2020.153129.
[6] Nimra Javed, Azam, Muhammad Awais, Ibrahim Qazi, Y. Amin, Hannu Tenhunen, Data-dense chipless RFID multisensor for aviculture industry, IEEE Microw. Wireless Compon. Lett. (2020) 1–4, https://doi.org/10.1109/LMWC.2020.3032027.
[7] Md Amin, Nemai Karmakar, Development of a chipless RFID temperature sensor using cascaded spiral resonators, IEEE Sensors (2011) 554–557, https://doi.org/10.1109/ICSENS.2011.6127344.
[8] Y. Feng, L. Xie, Q. Chen, L.R. Zheng, Low-cost printed chipless RFID humidity sensor tag for intelligent packaging, IEEE Sensor. J. 15 (6) (Jun. 2015) 3201–3208.
[9] M. Philipose, J.R. Smith, B. Jiang, A. Mamishev, R. Sumit, K. Sundara-Rajan, Battery-free wireless identification and sensing, IEEE Pervasive Comput. Mag. 4 (1) (Jan.–Mar. 2005) 37–45.
[10] A. Vena, L. Sydänheimo, M.M. Tentzeris, L. Ukkonen, A fully inkjet printed wireless and chipless sensor for CO2 and temperature detection, IEEE Sensor. J. 15 (1) (Jan. 2015) 89–99.
[11] Y.S. Chen, T.Y. Jiang, F.P. Lai, Design rule development for frequency-coded chipless radiofrequency identification with high capacity, IET Microw., Antennas Propag. 13 (2019) 1255–1261.
[12] Z. Xiao, et al., An implantable RFID sensor tag toward continuous glucose monitoring, IEEE J. Biomed. Health Inf. 19 (3) (May 2015) 910–919.
[13] S. Ali, S. Qaisar, H. Saeed, et al., Network challenges for cyber physical systems with tiny wireless devices: a case study on reliable pipeline condition monitoring, Sensors 15 (4) (2015) 7172–7205.
[14] S. Lyu, Y. Zhang, W. Wang, et al., Simulation study on influence of natural gas pipeline pressure on jet fire//IOP conference series: earth and environmental science, IOP Publishing 242 (2) (2019) 022041.
[15] X.N. Bui, H. Nguyen, H.A. Le, et al., Prediction of blast-induced air over-pressure in open-pit mine: assessment of different artificial intelligence techniques, Nat. Resour. Res. (2019) 1–21.
[16] Z. Chen, Z. Wang, X. Li, et al., Flexible piezoelectric-induced pressure sensors for static measurements based on nanowires/graphene heterostructures, ACS Nano 11 (5) (2017) 4507–4513. R. Bhattacharyya, C. Floerkemeier, and S. Sarma, "Towards tag antenna based sensing—An RFID displacement sensor," in Proc. IEEE Int. Conf. RFID, Orlando, FL, 2009, pp. 95–102.
[17] Z. Chen, Z. Wang, X. Li, et al., Flexible piezoelectric-induced pressure sensors for static measurements based on nanowires/graphene heterostructures, ACS Nano 11 (5) (2017) 4507–4513.
[18] S.C.B. Mannsfeld, B.C.K. Tee, R.M. Stoltenberg, et al., Highly sensitive flexible pressure sensors with microstructure rubber dielectric layers, Nat. Mater. 9 (10) (2010) 859.
[19] M. Zomorrodi, N.C. Karmakar, Cross-RCS based, high data capacity, chipless RFID system, in: 2014 IEEE MTT-S International Microwave Symposium (IMS2014), Tampa, FL, USA, 2014, pp. 1–4, https://doi.org/10.1109/MWSYM.2014.6848402.
[20] Hossam Abbas, Haythem Abdullah, Mahmoud Mohana, Hala Mansour, Gehan Shehata, High RCS Compact Orientation Independent Chipless RFID Tags Based on Slot Ring Resonators, SRR), 2018, pp. 69–76, https://doi.org/10.1109/NRSC.2018.8354361.
[21] A. Habib, et al., Data dense chipless RFID tag with efficient band utilization, AEU-Int. J. Elect. Communicat. (2022) 154220.
[22] H. Shahid, M.A. Riaz, A. Akram, J. Amin Y Loo, et al., Novel QR-incorporated hipless RFID tag, IEICE Electron. Express 16 (2019), 20180843- 20180843.
[23] Wazie Abdulkawi, Abdel Fattah Sheta, Khaled Issa, Saleh Alshebeili, Compact printable inverted-M shaped chipless RFID tag using dual-polarized excitation, Electronics 8 (2019) 580, https://doi.org/10.3390/electronics8050580.
[24] Iqra Jabeen, Asma Ejaz, Adeel Akram, Y. Amin, Jonathan Loo, Hannu Tenhunen, Y. Amin, Elliptical slot based polarization insensitive compact and flexible chipless RFID tag, Int. J. RF Microw. Computer-Aided Eng. (2019), https://doi.org/10.1002/mmce.21734.
[25] Amjad Ali, Orla Williams, Lester, Steve Greedy, High Code Density and Humidity Sensor Chipless RFID Tag, 2022, https://doi.org/10.23919/SpliTech55088.2022.9854366.
[26] Tehmina, Ameer Khan, Y. Amin, Shakeel Ahmad, RFID in IoT, miniaturized pentagonal slot-based data dense chipless RFID tag for IoT applications, Arabian J. Sci. Eng. 47 (2021), https://doi.org/10.1007/s13369-021-06228-9.
[27] Bilal Aslam, Azam, Muhammad Awais, Y. Amin, Jonathan Loo, Hannu Tenhunen, A high-capacity tunable retransmission type frequency coded chipless radio frequency identification system, Int. J. RF Microw. Computer-Aided Eng. 29 (2019) e21855, https://doi.org/10.1002/mmce.21855.
[28] Ameer Khan, Muhammad Riaz, Humayun Shahid, Y. Amin, Hannu Tenhunen, Jonathan Loo, Design of a cobweb shape chipless RFID tag, Microw. J. 64 (2021) 90.
[29] Nimra Javed, Azam, Muhammad Awais, Y. Amin, Chipless RFID multi-sensor for temperature sensing and crack monitoring in an IoT environment, IEEE Sensors Letters (2021), https://doi.org/10.1109/LSENS.2021.308321, 1-1.
[30] Yuan Gao, Mahboobeh Mahmoodi, Reza Zoughi, Design of a novel frequency-coded chipless RFID tag, IEEE Open J. Instrument. Measurem. 1 (2022), https://doi.org/10.1109/OJIM.2022.3175249, 1-1.
[31] Ameer Khan, Yassin Abdullah, Sidra Farhat, Wasim Nawaz, Usman Rouf, Design and Analysis of Truncated Elliptical Shaped Chipless RFID Tag, Turkish J. Elect. Eng. Computer Sci. (2020).
[32] F. Babaeian, N.C. Karmakar, A Semi-omnidirectional Resonator for Chipless RFID Backscattered Tag Design. 2020 27th International Conference on Telecommunications (ICT), 2020.
[33] S. Habib, A. Ali, G.I. Kiani, W. Ayub, S.M. Abbas, M.F.U. Butt, A low-profile FSS-based high capacity chipless RFID tag for sensing and encoding applications, Int. J. Microwave Wireless Technol. (2021) 1–9, https://doi.org/10.1017/S1759078721000362.
[34] N. Tariq, M.A. Riaz, H. Shahid, M.J. Khan, M.S. Khan, Y. Amin, J. Loo, H. Tenhunen, Orientation independent chipless RFID tag using novel trefoil resonators, IEEE Access 7 (2019) 122398–122407.
[35] N. Chen, Y. Shen, G. Dong, S. Hu, Compact scalable modeling of chipless RFID tag based on high-impedance surface, IEEE Trans. Electron. Dev. 66 (1) (Jan. 2019) 200–206, https://doi.org/10.1109/TED.2018.2864623.
[36] N. Javed, M.A. Azam, I. Qazi, Y. Amin, H. Tenhunen, Data-dense chipless RFID multisensor for aviculture industry, IEEE Microw. Wireless Compon. Lett. 30 (12) (Dec. 2020) 1193–1196, https://doi.org/10.1109/LMWC.2020.3032027.
[37] Hairong Kou, Qiulin Tan, Yi Wang, Guangjin Zhang, Shujing Su, Jijun Xiong, A wireless slot-antenna integrated temperature-pressure-humidity sensor loaded with CSRR for harsh-environment applications, Sensor. Actuator. B Chem. 311 (2020) 127907, https://doi.org/10.1016/j.snb.2020.127907.
[38] L. Shahid, H. Shahid, M.A. Riaz, S.I. Naqvi, M. Jamil, et al., Chipless RFID tag for touch event sensing and localization, IEEE Access 8 (2019) 502–513.
[39] I. Jabeen, A. Ejaz, M. Rehman, M. Naghshvarianjahromi, M. Khan, Y. Amin, J. Loo, H. Tenhunen, Data-dense and miniature Chipless moisture sensor RFID tag for Internet of Things, Electronics 8 (10) (2019) 1182, https://doi.org/10.3390/electronics810118.
[40] Y.S. Chen, T.Y. Jiang, F.P. Lai, Design rule development for frequency-coded chipless radiofrequency identification with high capacity, IET Microw., Antennas Propag. 13 (2019) 1255–1261.
[41] M. Tanzeel Khalid, A. Habib, M. Nadeem, Mir Yasir Umair, nimra javed, "printed humidity sensor for low-cost item tagging", AEU - Int. J. Elect. Communicat. 157 (154441) (2022) https://doi.org/10.1016/j.aeue.2022.154441. ISSN 1434-8411.

[42] Mehedi Noman, Usman Haider, Hidayat Ullah, Farooq Tahir, Hatem Rmili, Ali Najam, A 32-bit single quadrant angle- controlled chipless tag for radio frequency identification applications, Sensors 22 (2022) 2492, https://doi.org/10.3390/s22072492.
[43] M.S. Hashmi, V. Sharma, Design, analysis, and realization of chipless RFID tag for orientation independent configurations, Eng. J. 2020 (5) (Jan. 2020) 189–196.
[44] Usman Haider, Muhammad Noman, Aamir Rashid, Hatem Rmili, Hidayat Ullah, Farooq Tahir, A semi-octagonal 40- bit high capacity chipless RFID tag for future product identification, Electronics 12 (2023) 349, https://doi.org/10.3390/electronics12020349.
[45] F. Costa, S. Genovesi, A. Monorchio, Normalization-free chipless RFIDs by using dual-polarized interrogation, IEEE Trans. Microw. Theor. Tech. 64 (2016) 310–318.
[46] Hafsa Anam, Ayesha Habib, Irum Jafri, Y. Amin, Hannu Tenhunen, Directly printable frequency signatured chipless RFID tag for IoT applications, Radioengineering 26 (2017), https://doi.org/10.13164/re.2017.0139.
[47] N. Javed, A. Habib, Y. Amin, et al., "Miniaturized Flexible Chipless RFID Tag for IoT Market", International Conference on Communication, Computing and Digital Systems, C-CODE), 2017, pp. 71–74.
[48] L. Sevgi, Z. Rafiq, I. Majid, Radar cross section (RCS) measurements [testing ourselves], IEEE Antenn. Propag. Mag. 55 (6) (Dec. 2013) 277–291.
[49] N.C. Karmaker, Tag, you're it radar cross section of chipless RFID tags, IEEE Microw. Mag. 17 (7) (Jul. 2016) 64–74, https://doi.org/10.1109/MMM.2016.2549160.
[50] R.B. Dybdal, Radar cross section measurements, Proc. IEEE 75 (4) (Apr. 1987) 498–516, https://doi.org/10.1109/PROC.1987.13757.
[51] M. Grace, Measurement of Radar Cross Section Using the 'VNA Master' Handheld VNA: Application Note, Anritsu, Atsugi, Japan, 2011.
[52] A. Vena, E. Perret, S. Tedjini, Chipless RFID tag using the hybrid coding technique, IEEE Trans. Microw. Theor. Tech. 59 (12) (2011) 3356–3364.
[53] M. Polivka, M. Svanda, J. Havlicek, J. Machac, Detuned dipole array backed by rectangular plate applied as chipless RFID tag, in: Proc. Prog. Electromagn. Res. Symp, .-Spring (PIERS), St, Petersburg, Russia, May 2017, pp. 3314–3317, https://doi.org/10.1109/PIERS.2017.8262328.
[54] S.K. Behera, N.C. Karmakar, Chipless RFID printing technologies: a state of the art, IEEE Microw. Mag. 22 (6) (June 2021) 64–81, https://doi.org/10.1109/MMM.2021.3064099.
[55] M.A. Islam, N.C. Karmakar, Real-world implementation challenges of a novel dual-polarized compact printable chipless RFID tag, IEEE Trans. Microw. Theor. Tech. 63 (12) (Dec. 2015) 4581–4591, https://doi.org/10.1109/TMTT.2015.2495285.
[56] J.F. Salmerón, A. Albrecht, S. Kaffah, M. Becherer, P. Lugli, A. Rivadeneyra, Wireless chipless system for humidity sensing, Sensors 18 (7) (2018) 2275. https://doi:10.3390/s18072275.
[57] N. Javed, A. Habib, Y. Amin, J. Loo, A. Akram, H. Tenhunen, Directly printable moisture sensor tag for intelligent packaging, IEEE Sensor. J. 16 (16) (2016) 6147–6148. https://doi:10.1109/JSEN.2016.2582847.
[58] Kapton®HN Polyimide Film Datasheet. Available online: http://www2.dupont.com/Kapton/en_US/(accessed on 18 September 2011).